Nanoscale Electrical Conductivity and Surface Spectroscopic Studies of Indium−Tin Oxide

Yish-Hann Liau and Norbert F. Scherer*

Department of Chemistry, The James Franck Institute, and Materials Research Science and Engineering Center, University of Chicago, 5735 S. Ellis Ave., Chicago, Illinois 60637

Kent Rhodes

McCrone Associates, 850 Pasquinelli Dr., Westmont, Illinois 60559

Received: November 7, 2000; In Final Form: January 31, 2001

Optically transparent indium−tin oxide (ITO) is a "universal" electrode for various optoelectronic devices such as organic light emitting diodes (OLEDs). It is known that the performance of OLEDs improves significantly by exposing the ITO surface to an oxygen plasma. This study employs conducting atomic force microscopy (C-AFM) for unique nanometer-scale mapping of the local current density of a vapor-deposited ITO film. The local conductance is shown to increase by orders of magnitude and becomes more uniform after oxygen plasma treatment for measurements of the identical 200-nm^2 regions. Scanning tunneling microscopy (STM) and X-ray photoelectron spectroscopy measurements of separate regions of the same films suggest that the oxygen plasma removes a thin layer of insulating carbon-rich material from the surface. The extensive heterogeneity in interfacial electrical conductivity measured by C-AFM calls into question previous studies of STM-induced electroluminescence of polymer films on ITO as well as STM imaging of such films. The impact of this study on the future development of optoelectronic devices is discussed.

I. Introduction

Tin-doped indium oxide (ITO) is routinely used as an electrode in various optoelectronic devices such as flat panel displays, solar cells, and organic electroluminescence devices due to its unique combination of properties, including high optical transparency, low electrical resistance, and excellent surface adhesion.[1] The nonstoichiometric nature of ITO leads to intrinsic heterogeneity of the same properties. The surface electronic properties that determine interfacial charge transport are affected by the chemical compositions. The spatial heterogeneity of the surface electronic structure of ITO, in turn, limits the performance of optoelectronic devices constructed with ITO electrodes. Therefore nanometer-scale measurement of ITO's surface electronic (i.e., *I*/*V*) characteristic is essential to reveal the heterogeneity.

Research into and commercialization of polymer-based organic light emitting devices (OLEDs) has been extensive in the past decade because of the promise of being the basis for a low-cost, easy-to-process, structurally flexible alternative to traditional LEDs.[2−9] However, OLEDs made with ITO electrodes are usually less efficient and lack long-term stability and reproducibility in manufacture compared with semiconductor-based LEDs. Inefficient hole-injection and low hole mobility have been proposed to partially account for low emission efficiencies and the high driving bias required for operation in single-layer devices.[2,4,10−13] One approach used to improve performance is to add a hole-transport or -injection layer between the ITO electrode and the emitting medium to increase the probability of electron/hole recombination occurring within the emitting medium.[13,14] Also, various treatments of the ITO surface have been reported that decrease the "turn-on" voltage.[15−25] Notably, a significant improvement in the performance of OLED devices achieved by exposing the ITO surface to an oxygen plasma has been reported.[15,17,19,21,25] However, most of the previous studies have been limited to a macroscopic (i.e., large area averaged) measurement and have not given direct microscopic evidence for the changes that occur.

Recently, scanning tunneling microscopy (STM) has been used in electroluminescence studies of OLEDs in which the tip served as a nanometer-scale electrode.[26−29] The STM tip height and the luminescence intensity recorded in a point-by-point fashion were used to generate correlated topographic and photon emission maps. The electroluminescence was found to be highly nonuniform on the nanometer scale, and the emitting region constituted only a small portion of the whole scanning area.[29] Although the origin of the heterogeneity in the spatially resolved emission is not clear, the heterogeneity in the electronic properties of the ITO surface is almost certainly a factor. Reducing the nonuniformity and increasing the charge injection efficiency will improve the performance of OLEDs as well as other optoelectronic devices that are comprised of ITO electrodes.

This paper presents the results of electrically conducting atomic force microscopy studies of oxygen plasma treated ITO surfaces. Unique information about the influence of oxygen plasma treatment on the local electronic properties is obtained by measuring the conductance in the identical submicron region with better than 20 nm spatial registration of "before" and "after" plasma treatment of the sample. Local $I-V$ characteristics are measured and are analyzed by the Fowler−Nordheim field emission model of electron tunneling to extract the thickness of the insulating layer. Further, X-ray photoelectron spectros-

* To whom correspondence should be addressed. E-mail: nfschere@uchicago.edu.

10.1021/jp0040749 CCC: $20.00
Published on Web 03/23/2001

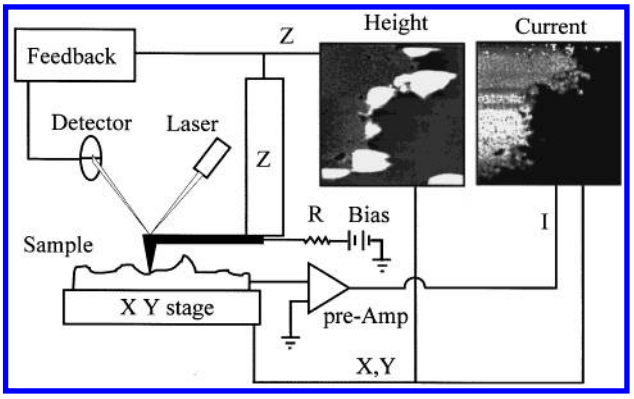

Figure 1. Experimental setup for correlated C-AFM topography and conductance imaging. A commercial AFM is mounted on an optical inverted microscope. The sample is raster scanned relative to the AFM tip by a closed-loop XY stage. The AFM is operated in constant force mode where the tip height and the current are recorded in a point-by-point fashion to generate topography and conductance maps. The topography and current images (scan area: 2 by 2 μm) are actual results for Au films on glass. The film thickness is 30 nm as measured from the substrate to the plateau area. The full scale of the current image is 1.5 nA.

copy is used to identify the elemental content of the surface "layer" that creates the electrical heterogeneity.

II. Experimental Section

The ITO-coated cover glass slips (Thin Film Devices Inc.) used in this study have a sheet resistance of 20 Ω/□ as specified by the vendor. The ITO samples were cleaned by a standard degreasing method including repeated rinsing with acetone and deionized water, and then dried in a vacuum oven.[15] The samples were analyzed after primary cleaning (termed "as received" samples) and after treatment in an oxygen plasma (Plasmod, March Instruments, Inc.) for 2 min at an oxygen pressure of ~1 Torr and a plasma power of 50 W (termed "plasma treated" samples).

A schematic of the scanning probe experimental setup is shown in Figure 1. The home-built conducting probe atomic force microscope (C-AFM) is based on a commercial AFM (Digital Instruments, Bioscope). The C-AFM is mounted on top of an inverted optical microscope (Zeiss, Axiovert 100) for simultaneous optical and scanning probe imaging of the same region of the sample surface. The sample is positioned in *x* and *y* with a closed-looped scanning stage (Queensgate, NPS-XY-100A) with ~1 nm scanner reproducibility over the 100 μm scan range. The combination of far-field optical microscopy and the "dual" scanning capabilities (tip or sample scan) facilitate repositioning the sample and imaging the same area with nanometer-scale reproducibility provided that position reference markers can be identified. The reproducibility is essential in this study because oxygen plasma treatment requires removing the sample from the microscopy apparatus.

A bias voltage is applied to the silicon cantilevers (Silicon-MDT, CSC12/TiN) that are coated with a layer of conductive titanium nitride to provide electrical contact with the sample. The force constant of the cantilever is 0.6 N/m as specified by the manufacturer. A glass cantilever holder is used to insulate the cantilever from the AFM electrical circuits (e.g., the PZT drive). The current was measured from the sample and converted to a voltage with a high-impedance current amplifier (Femto, LCA-4K-TG). A 10 MΩ resistor was used in the circuit to limit the current. A variable low-pass filter was used to reduce the electrical noise. The whole setup is in a temperature-controlled room enclosed in an acoustic and electromagnetic-isolated, dry nitrogen purged box to reduce environmental influences on the measurements. The AFM is operated in contact mode with an applied force of ~12 nN, and the tip height is measured simultaneously along with the current to generate correlated topography and conductance images of the same region. The peak-to-peak noise level is 15 pA for a 10 ms/point integration time for conductance map images and 5 pA for *I*−*V* measurements where a longer integration time and a smaller RC constant are employed (100 ms and 30 Hz, respectively).

The X-ray photoelectron spectroscopy (XPS) experiments were performed in a Physical Electronics Quantum 2000 instrument. The analyses were conducted at a pressure of less than 1×10^{-8} Torr. The specimens were irradiated with monochromatic Al Kα X-rays at an energy of 1486.6 eV. The X-ray beam diameter is about 100 μm; hence, these measurements integrate over the electrically heterogeneous regions observed in C-AFM and do not allow spatially resolved spectroscopic characterization.

Survey spectra were collected from five, ~2 mm^2 areas at a constant pass energy of 187 eV. High-resolution spectra of carbon, oxygen, indium, and tin were collected from multiple, 50−100 μm areas using pass energies of 23.5 or 11.8 eV. All binding energies were referenced to the Ag $3d_{5/2}$ line at 386.26 eV. Sample charging was not detected on any of the samples. The elemental compositions of the samples, in atomic concentrations, were determined using relative sensitivity factors measured from standards.[30,31] The high-resolution carbon, oxygen, indium, and tin spectra were analyzed using curve-fitting techniques to identify multiple chemical species, and to determine peak positions.[32,33] The component peak parameters were constrained to physically realistic values based on measurements of oxide standards.[33]

III. Results and Discussion

C-AFM Images and *I/V Characteristics.* A gold film deposited on a glass substrate was imaged to test the C-AFM apparatus; a small part of the gold film was scratched off to expose the glass underneath. The topographic image (shown in Figure 1) clearly resolves the "interface" with the scratched region being lower than the region where the film is intact. The current image of the same region is well correlated with the location of the Au film and bare glass. Current−voltage measurements in the conductive region exhibit linear (ohmic) behavior defined by the circuit resistance.

Topographic and conductance images of the solvent-cleaned ITO surface are shown in Figure 2. The AFM image (Figure 2a) shows grainy features that are typical for "polycrystalline" ITO with a domain size of about 70 nm. The simultaneously acquired conductance image is displayed in Figure 2b. The current density map does not correlate with the grainy features of the ITO surface; while some grains appear to be nearly electrically insulating (the features on the left part of the AFM image), other grains exhibit both highly and poorly conductive regions.

To quantify the variation of the local conductance, a series of *I*−*V* curves were measured at equally spaced points along a horizontal line (white solid line in Figure 2). The results are shown in Figure 3. The resistance values are derived from the slope about the origin of the voltage axis. The resistance in the highly conductive region is negligibly smaller than the 10 MΩ limiting resistance of the circuit. *Resistance values 4 orders of magnitude larger, limited by the range of the preamplifier used in the experiment, are observed only 20 nm separated from*

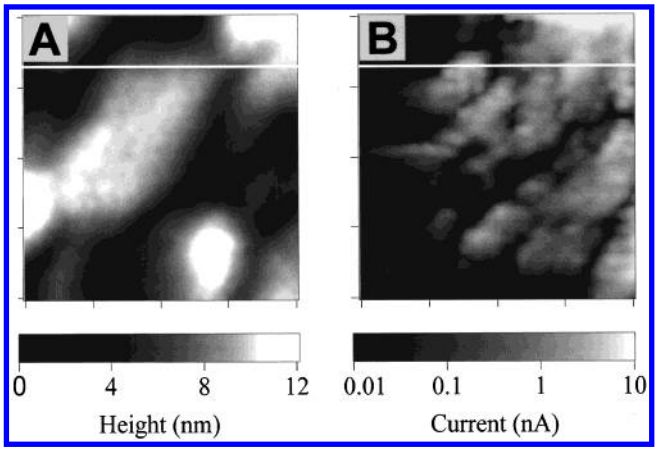

Figure 2. Topography (a) and simultaneously acquired conductance (b) images of ITO. Scan area: 200 by 200 nm. The path where the local $I-V$ measurements were performed is indicated by the solid white lines.

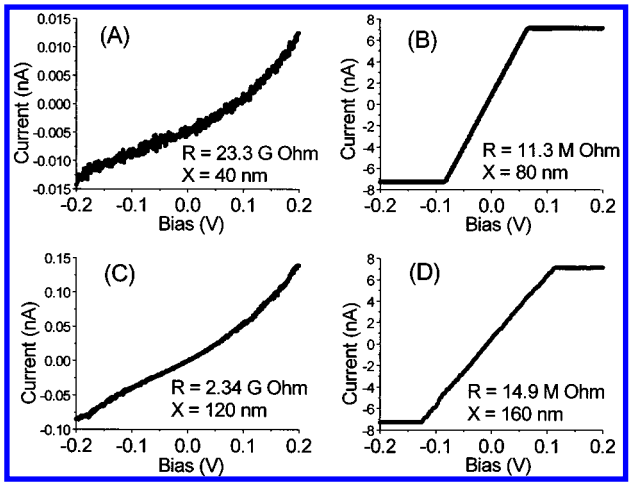

Figure 3. Selected and representative localized $I-V$ characteristics measured at different positions along the white line in Figure 2. The x-coordinate of the measured position and the resistance are labeled in each panel.

regions of ohmic conductivity. Also, nonlinear $I-V$ curves are observed in the low conductance regions.

Plasma-Treated Films. To study the influence of the oxygen plasma treatment, the ITO films are marked by carefully scratching the surface with a diamond cutter. The scratch, about 1 μm in width and visible with the optical microscope, serves as spatial reference allowing the sample to be repositioned to the same position for AFM scanning. Topographic and conductance images were taken in an area several tens of microns away from the scratch to avoid any possible influence of mechanical stress introduced by scratching. After imaging the untreated film (topography and current images in parts a and b, respectively, of Figure 4), the sample was exposed to an oxygen plasma under conditions similar to those reported to have improved the performance of OLEDs.[15] The topographic and conductance imaging was performed immediately after oxygen plasma treatment. The corresponding results for the plasma treated surface are shown in Figure 4c,d where the topography is largely unchanged (compare Figure 4a,c) but the conductance has increased more than 10-fold and has become more uniform. The high end of the conductance scale in Figure 4d reflects ohmic behavior as judged from the associated $I-V$ characteristics (not shown).

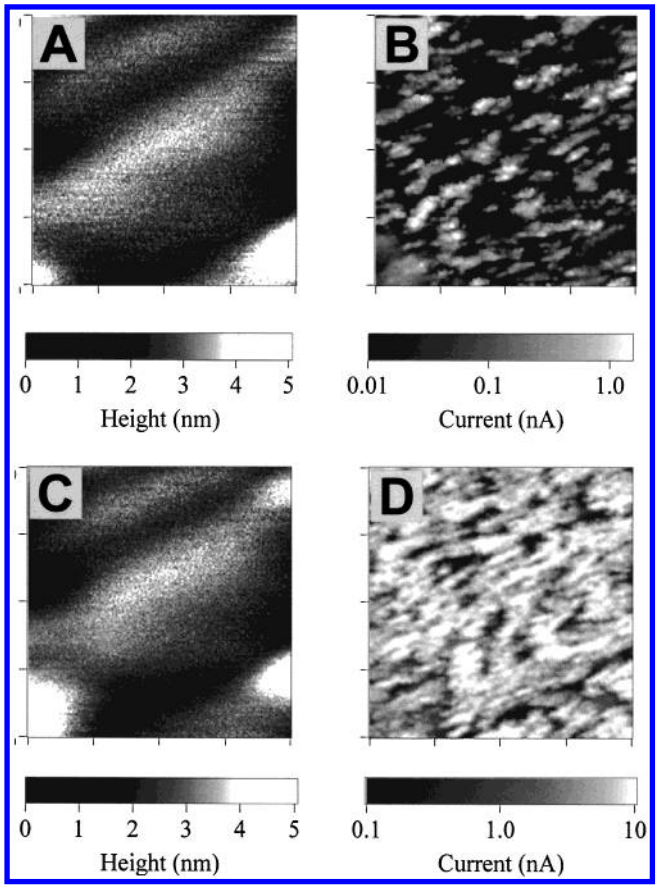

Figure 4. Topography and conductance images of the identical region of an ITO thin film measured before and after exposing the sample to the oxygen plasma. Scan area: 200 by 200 nm. Topography (a) and conductance (b) are before oxygen plasma etching, and (c) and (d) are measured after plasma etching.

Fowler−Nordheim Analysis. In the low conductivity area of the ITO surface, the contaminating (e.g., organic) layer prevents the formation of an ohmic contact between the ITO and the conducting cantilever at an applied force of 12 nN. If the insulating layer is thin enough, the electrons can tunnel through the barrier under bias and reach the other electrode. The Fowler−Nordheim field emission model is used to gain further insight into the electron transport mechanism. The current tunneling through a metal−oxide−semiconductor parallel junction is[34]

$$I = A_{\text{eff}}\frac{e^3}{8\pi h\phi}\left(\frac{V}{s}\right)^2 \exp\left(-\frac{8\pi\sqrt{2m}}{3he}\frac{\phi^{3/2}s}{V}\right)$$

where A_{eff} is the effective emission area, e is the electron charge, h is Planck's constant, s is the oxide thickness, ϕ is the barrier height, V is the bias across the junction, and m is the electron mass. The actual emission area and the Z-dependence of electron collection depend on the tip shape; its determination is beyond the scope of this paper. In addition, neither the barrier height nor the insulator thickness is known independently. Obviously, an $I-V$ measurement cannot uniquely determine all of these parameters. However, a reasonable fit to the $I-V$ measurement with this field emission tunneling model can be obtained in the case of the low conductivity regions. Figure 5 shows the result of nonlinear curve fitting of a data set corresponding to the negative bias side of Figure 3a (i.e., electrons tunnel from the tip to the ITO surface). The signs of the current and the voltage have been reversed in concordance with the formula. The result

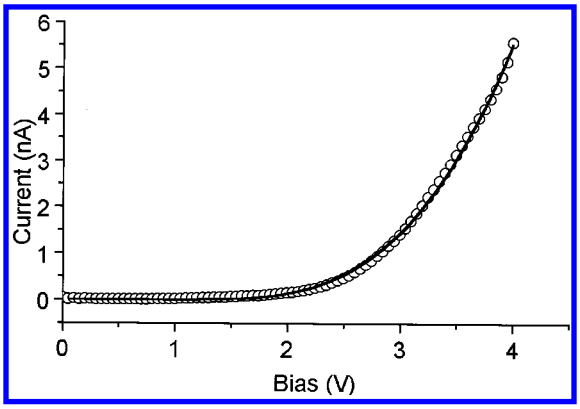

Figure 5. Fowler−Nordheim model best fit to the $I-V$ curve of an insulated region of an ITO film. Data are shown as open circles, and the best fit is displayed as a solid curve.

of the best-fit shows $A_{eff}/\phi s^2$ and $s\phi^{3/2} = 19.3$. The work function of the TiN conducting coating is 3.74 eV,[35] and that of ITO is 4.4−4.5 eV.[36] If the barrier is assumed to be 3.74 eV, the insulator thickness and the effective emission area was found be 2.7 and 27 nm^2, respectively. The estimated emission area is reasonable as compared to the known tip size and geometry. The insulator thickness is larger than expected from the crude estimates that can be made by comparing C-AFM and STM results (see next subsection). No physically reasonable set of fitting parameters can be obtained in the higher conductivity regions indicating that direct ohmic contact rather than tunneling is a more suitable description of the conductance.

Scanning secondary ion mass spectrometry (SIMS) measurements of solvent and plasma-cleaned films were performed. The measurements were not able to resolve significant differences between the "before" and "after" samples. Although this is a negative result, it is consistent with the idea that the organic insulating film is very thin, and was perhaps quickly removed by the destructive/ablative SIMS method.

Comparison to STM. ITO samples without plasma treatment were examined by scanning tunneling microscopy (STM) in constant current mode. The images (not shown) resemble those of Figure 4a or 4c. The root-mean-square roughness values obtained from STM and AFM topographic images of equal area and pixel resolution (e.g., 1 μm^2 region divided into 512-by-512 pixels) are almost identical. Still, the imaging and feedback modalities are entirely different. In constant current mode, the STM continues to apply force to (i.e., push) the tip into the sample until a sufficiently good contact is made so that the set-point current (∼1 nA) can flow through the circuit. In contrast, the conducting AFM measurements use the interaction force between the sample and the cantilever tip (hence cantilever deflection) as a feedback mechanism. Therefore, one has to conclude that the STM was "scraping away" the very thin (a few nanometers at most) inhomogeneous "insulating" layer.

X-ray Photoelectron Spectroscopy. Representative XPS survey spectra for ITO films as received and after treatment by oxygen plasma are shown in Figure 6. The surface atomic compositions of the films, averaged over five different areas, are listed in Table 1. Changes in atomic composition on ITO surfaces due to plasma etching have been proposed to explain the reduced "turn-on" voltage in OLED devices.[15,37] The present results, summarized in Table 2, show that the In:Sn ratio of 5.5 does not change with plasma treatment, while the (In,Sn):O ratio changes only from 0.55 to 0.58 with plasma treatment. The ratios are very consistent in the multiple analysis areas (relative standard deviation < 5%). Consequently, the minor

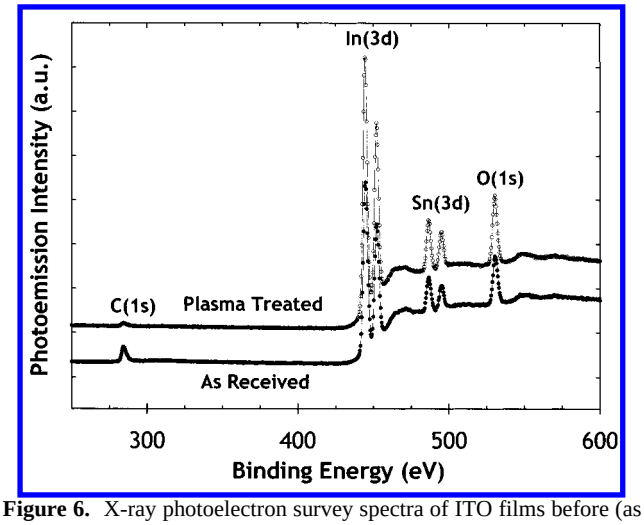

Figure 6. X-ray photoelectron survey spectra of ITO films before (as received) and after (plasma treated) 2 min treatment in a 50 W oxygen plasma. Before plasma etching (light curve) and after (dark curve).

TABLE 1: Surface Elemental Composition of ITO Films[a]

	atomic percentage	
	as received	plasma treated
oxygen	43.0 ± 0.5	56.8 ± 1.4
carbon	31.0 ± 0.9	6.2 ± 0.9
indium	19.6 ± 0.2	27.0 ± 0.4
tin	3.5 ± 0.1	4.8 ± 0.1
copper	1.1 ± 0.3	1.7 ± 0.2
nitrogen	0.7 ± 0.6	0.4 ± 0.2
zinc	0.5 ± 0.1	0.6 ± 0.1
sulfur	0.4 ± 0.3	0.9 ± 0.2
silicon	<0.5	1.6 ± 0.7
total	100.0	100.0

[a] Results are the normalized averages from survey measurements of five, ∼2 mm^2 areas ±1σ uncertainties.

TABLE 2: Atomic Ratios and Indium and Tin Peak Positions[a]

	atomic ratios		binding energy (eV ± 1σ)	
sample	In:Sn	(In,Sn):O	In 3d$_{5/2}$	Sn 3d$_{5/2}$
as received	5.5 ± 0.2	0.55 ± 0.02	444.83 ± 0.03	486.95 ± 0.03
plasma treated	5.5 ± 0.1	0.58 ± 0.02	444.76 ± 0.03	486.82 ± 0.03

[a] Atomic ratios are reported with 1σ uncertainties from 10 measurement areas. Binding energies are referenced to Ag 3d$_{5/2}$ at 386.26 eV and reported with 1σ uncertainties.

change in atomic composition of In and Sn cannot account for the several orders of magnitude increased conductance observed by C-AFM.

By contrast, the carbon concentration on the surface of the ITO films decreases from 31% to 6% after oxygen plasma treatment. Figure 7 shows representative carbon XPS spectra of the as received and oxygen plasma treated films. The carbon peaks determined by curve fitting are consistent with C−C and C−O bonding typical of organic contamination.[30] Assuming a uniform, organic surface film, the ratios of carbon and indium peak intensities correspond to a contamination film thickness of 2.2 ± 0.2 and 0.5 ± 0.1 nm for the as received and the oxygen plasma treated ITO films, respectively.[30,38] This is in good agreement with results of the Fowler−Nordheim analysis given above. Oxygen plasma treatment very effectively removes the insulating organic layer and would explain the larger and more uniform conductance observed by C-AFM. By comparison, the standard degreasing method is not sufficient to do the same. This thin layer of adventitious carbon is common on all

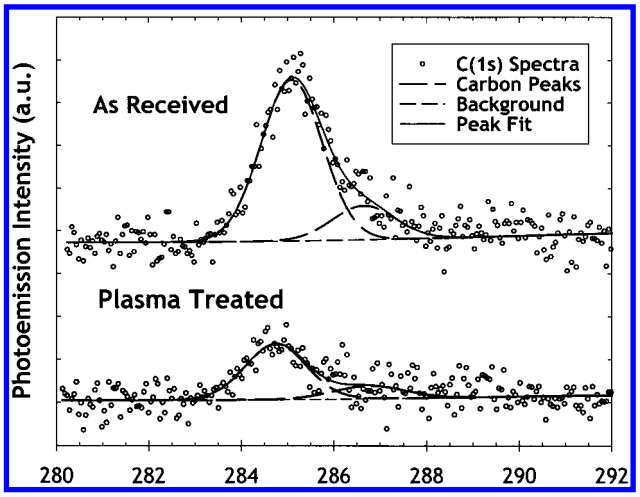

Figure 7. Carbon 1s XPS spectrum of as received and plasma treated ITO films. The spectra were curve fit with two Gaussian−Lorentzian sum peaks and a Tougaard background function.

air-exposed surfaces, and is difficult to remove with solvent-based cleaning techniques.[38,39]

Parts a and b of Figure 8 show oxygen XPS spectra of the as received and oxygen plasma treated films, respectively. The as received spectrum versus the oxygen plasma treated difference spectrum is shown in Figure 8c, and curve-fitting results are reported in Table 3. Four oxygen (Gaussian shape) peaks, with similar widths and positions, were used to fit the O(1s) XPS peak envelopes in all the samples. These peaks are listed as peaks O_I through O_{IV} in Table 3. These peak assignments are in good agreement with previous XPS analyses of ITO films.[39,40] Peak O_I, at a binding energy of 530 eV, appears only after oxygen plasma treatment. Formation of this species was reported in a previous study.[25] Peak O_{II} has a binding energy consistent with the oxides In_2O_3 and SnO_2 (O_2 bound to In_3^+ and Sn_4^+, respectively), whereas peak O_{III} is consistent with the hydroxide $In(OH)_3$ (oxygen in −OH bonds).[31,39,41] Peak O_{IV}, at a binding energy of 533 eV, may be due to adsorbed water. It may also include oxygen in adsorbed organic contaminants, and oxygen from SiO_2.[39] Peaks O_I and O_{IV} are readily removed by argon ion sputtering, indicating they are primarily on the outer surface of the film.

A recent study of ITO surface treatments identified three factors affecting surface electrical properties: (1) removal of surface carbonaceous contamination, (2) changes in the In/Sn ratio indicative of the Sn dopant concentration, and (3) changes in the concentration of oxygen vacancies.[37] Another study proposed that ITO surface treatments, including oxygen plasma treatment, produces oxidation of Sn−OH surface groups to Sn−O• species.[25] The present C-AFM/STM comparisons and XPS measurements show that a thin, insulating layer of carbonaceous contamination is removed during oxygen plasma treatment. However, the elemental ratios measured by XPS before and after oxygen plasma treatment in this study show no change in Sn dopant concentration.

The remaining two factors, oxygen vacancy concentration and Sn−OH oxidation, will produce changes in oxygen−indium−tin ratios and O(1s) XPS spectra. If the O_I, O_{II}, and O_{III} oxygen peaks are assigned to oxygen in the ITO film, then the insignificant change in the $(O_I + O_{II} + O_{III})/(In + Sn)$ ratio (1.61 to 1.62) after oxygen plasma treatment indicates that oxygen is not being added to the film. The small change in overall $O/(In + Sn)$ ratio after oxygen plasma treatment can be explained by loss of oxygen from the organic contaminant film,

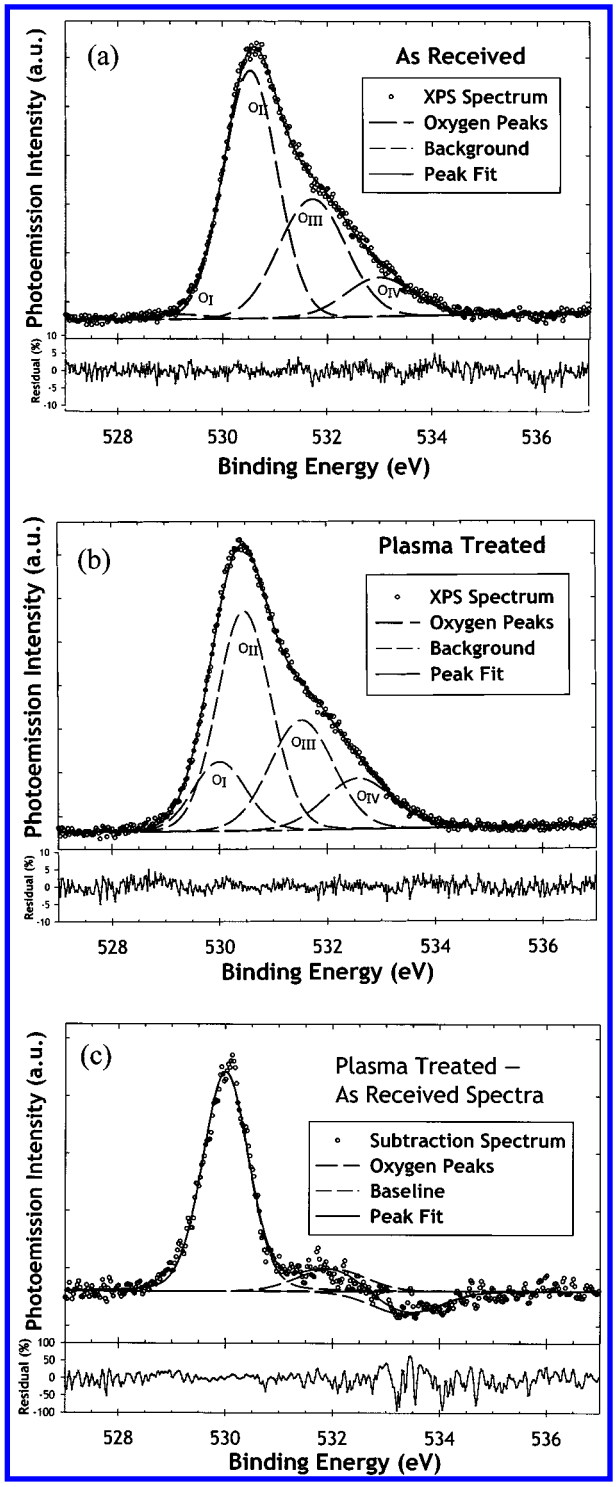

Figure 8. (a) Oxygen 1s XPS spectrum of as received ITO film. The spectrum was curve fit with four Gaussian−Lorentzian sum peaks and a Tougaard background function. (b) Oxygen 1s XPS spectrum of plasma treated ITO film. The spectrum was curve fit with four Gaussian−Lorentzian sum peaks, and a Tougaard background function. (c) Result of subtraction of as received O(1s) spectrum from plasma treated O(1s) spectrum. The spectrum was curve fit with three Gaussian−Lorentzian sum peaks and a Tougaard background function.

and possibly some loss of adsorbed water. Also, assignment of the higher binding energy O_{II} peak to lattice oxygen near vacancies implies an unreasonably large oxygen vacancy density in the film that decreases with oxygen plasma treatment.[39] Thus, the present XPS results do not support oxygen vacancy changes as a significant effect of oxygen plasma treatment.

TABLE 3: Oxygen 1s Curve Fitting Results[a]

		oxygen species			
sample	measurement	O_I	O_{II} oxide	O_{III} −OH	O_{IV} H_2O
as received	binding energy (eV)	529.5 ± 0.3	530.50 ± 0.03	531.71 ± 0.05	532.96 ± 0.07
	relative area (%)	<3	56 ± 5	32 ± 5	11 ± 3
plasma treated	binding energy (eV)	529.97 ± 0.05	530.47 ± 0.04	531.70 ± 0.04	532.92 ± 0.13
	relative area (%)	14 ± 2	49 ± 4	30 ± 3	7 ± 2
etched 10 nm	binding energy (eV)	529.7 ± 0.2	530.55 ± 0.03	531.72 ± 0.05	533.10 ± 0.13
	relative area (%)	<5	76 ± 5	18 ± 4	<4

[a] Binding energies are referenced to Ag $3d_{5/2}$ at 386.26 eV and reported with 1σ uncertainties. Relative areas are reported as relative percentages of the oxygen 1s peak area, reported with 1σ uncertainties

The last factor proposed as a mechanism for changing ITO surface electrical properties by oxygen plasma treatment is oxidation of Sn−OH surface groups to Sn−O• species.[25] Thus, the O_I XPS peak of Figure 8 would be assigned to the Sn−O• species. The O_I/Sn ratio of approximately 1.7 after oxygen plasma treatment is consistent with delocalization of excess electron density across multiple oxygen atoms, and accounts for the increase in the O_{III}/O_{II} peak ratio, since for each −OH bond oxidized, more than one O_{II} oxygen is shifted to the O_I peak. Thus, oxidation of Sn−OH surface groups to Sn−O• is consistent with the XPS results.

The peak positions of the In $3d_{5/2}$ and Sn $3d_{5/2}$ peaks decrease slightly after oxygen plasma treatment (Table 2). Further analysis of the multiple indium and tin peaks in the XPS spectra was not performed in part because they are less relevant to the present paper and have been more extensively examined in a recent mechanistic study.[40]

IV. Conclusions

Conducting atomic force microscopy is used to study the variation of the local interfacial conductance of ITO thin films before and after oxygen plasma etching. The oxygen plasma is effective in removing the insulating layer, thereby increasing the conductance and improving the uniformity, whereas standard (i.e., solvent-only) degreasing methods are not adequate for this purpose. The average local conductance increases more than 10-fold after the surface is exposed to the oxygen plasma. The force feedback mechanism of C-AFM measurements made the characterization possible; STM measurements are insensitive to the presence of an interface with highly heterogeneous conductivity. Comparisons of C-AFM and STM images and XPS measurements suggest that a thin, primarily organic hydrocarbon, insulating layer is removed during plasma etching.

Conclusions drawn from the present XPS measurements are that both removal of carbon contamination and surface hydroxide oxidation are possible mechanisms for increased conductivity of ITO films after oxygen plasma treatment. These conclusions are consistent with a recent XPS study on ITO[25] and the general ideas very recently put forth in mechanistic studies of ITO surface chemistry/reactivity.[40] The thickness of the carbon layer removed by oxygen plasma treatment, ∼1.7 nm, is in excellent agreement with the Fowler−Nordheim analysis of C-AFM *I*/*V* characteristics of the selected nanometer locations.

The results suggest one explanation for the improved performance of OLEDs following ITO plasma etching/cleaning. Plasma treatment increases the fraction of the ITO−polymer interface in OLEDs that achieves ohmic contact, thereby reducing the driving voltage required for luminescence or device turn on. This improvement in conductivity is obtained under plasma cleaning conditions that do not increase the ITO sample surface roughness on even the sub-nanometer scale. Hence, the uniformity of the ITO−polymer interface would not be degraded. This would not necessarily be true under significantly more vigorous plasma cleaning conditions that might further improve the uniformity of the interfacial conductivity.

Acknowledgment. This research was supported by the W. M. Keck Foundation (991705) and the University of Chicago MRSEC (DMR-9808595). N.F.S. acknowledges the Dreyfus Foundation for a fellowship. We thank Prof. Ricardo Levi-Setti, University of Chicago, Department of Physics, for the effort made in scanning SIMS studies of these films.

References and Notes

(1) Eisgruber, I.; Engel, J.; Hollingsworth, R.; Rhat, P. *Vacuum Thin Film Technol.* **1999**, *6*, 21−25.
(2) Tang, C. W.; Vanlyake, S. A. *Appl. Phys. Lett.* **1987**, *51*, 913−915.
(3) Burroughe, J. H.; Bragley, D. D. C.; Brown, A. R.; Marks, R. N.; Mackay, K.; Friend, R. H.; L., B. P.; B., H. A. *Nature* **1990**, *347*, 539−541.
(4) Sheats, J. R.; Antoniadis, H.; Hueschen, M.; Leonard, W.; Miller, J.; Moon, R.; Roitman, D.; A., S. *Science* **1996**, *273*, 884−888.
(5) Hide, F.; Diaz Garcia, M. A.; Schwartz, B. J.; Heeger, A. J. *Acc. Chem. Res.* **1997**, *30*, 430−436.
(6) Sirringhaus, H.; Tessler, N.; Friend, R. H. *Science* **1998**, *280*, 1741−1744.
(7) Campbell, I. H.; Davids, P. S.; Smith, D. L.; Barashkov, N. N.; Ferraris, J. P. *Appl. Phys. Lett.* **1998**, *72*, 1863.
(8) Kraft, A.; Grimsdale, A. C.; Holmes, A. B. *Angew. Chem.* **1998**, *37*, 402−428.
(9) Friend, R. H.; Gymer, R. W.; Holmes, A. B.; Burroughes, J. H.; Marks, R. N.; Taliani, C.; Bradley, D. D. C.; Dos Santos, D. A.; Bredas, J. L.; Logdlund, M.; Salaneck, W. R. *Nature* **1999**, *397*, 121−128.
(10) Greenham, N. C.; Moratti, S. C.; Bradley, D. D. C.; Friend, R. H.; Holmes, A. B. *Nature* **1993**, *365*, 628−630.
(11) Burrows, P. E.; Bulovic, V.; Forrest, S. R.; Sapochak, L. S.; McCarty, D. M.; Thompson, M. E. *Appl. Phys. Lett.* **1994**, *65*, 2922−2924.
(12) Parker, I. D. *J. Appl. Phys.* **1994**, *75*, 1656−1666.
(13) Yang, Y.; Westerweele, E.; Zhang, C.; Smith, P.; Heeger, A. J. *J. Appl. Phys.* **1995**, *77*, 694−698.
(14) Van Slyke, S. A.; Chen, C. H.; Tang, C. W. *Appl. Phys. Lett.* **1996**, *69*, 2160−2162.
(15) Wu, C. C.; Wu, C. I.; Sturm, J. C.; Kahn, A. *Appl. Phys. Lett.* **1997**, *70*, 1348−1350.
(16) Li, F.; Tang, H.; Shinar, J.; Resto, O.; Weisz, S. Z. *Appl. Phys. Lett.* **1997**, *70*, 2741−2743.
(17) Furukawa, K.; Terasaka, Y.; Ueda, H.; Matsumura, M. *Synth. Met.* **1997**, *91*, 99−101.
(18) Kim, J. S.; Granstrom, M.; Friend, R. H.; Johansson, N.; Salaneck, W. R.; Daik, R.; Feast, W. J.; Cacialli, F. *J. Appl. Phys.* **1998**, *84*, 6859−6870.
(19) Kim, J. S.; Friend, R. H.; Cacialli, F. *Appl. Phys. Lett.* **1999**, *74*, 3084−3086.
(20) Mason, M. G.; Hung, L. S.; Tang, C. W.; Lee, S. T.; Wong, K. W.; Wang, M. *Appl. Phys. Lett.* **1999**, *86*, 1688−1692.
(21) Steuber, F.; Staudigel, J.; Stossel, M.; Simmerer, J.; Winnacker, A. *Appl. Phys. Lett.* **1999**, *74*, 3558−3560.
(22) Tadayyon, S. M.; Griffiths, K.; Norton, P. R.; Tripp, C.; Popovic, Z. *J. Vac. Sci. Technol., A* **1999**, *17*, 1773−1778.
(23) Nuesch, F.; Rothberg, L. J.; Forsythe, E. W.; Le, Q. T.; Gao, Y. *Appl. Phys. Lett.* **1999**, *74*, 880−882.
(24) Choi, B.; Yoon, H.; Lee, H. H. *Appl. Phys. Lett.* **2000**, *76*, 412−414.

(25) Milliron, D. J.; Hill, I. G.; Shen, C.; Kahn, A.; Schwartz, J. *J. Appl. Phys.* **2000**, *87*, 572−576.
(26) Lidzey, D. G.; Bradley, D. D. C.; Alvarado, S. F.; Seidler, P. F. *Nature* **1997**, *386*, 135−135.
(27) Alvarado, S. F.; Riess, W.; Seidler, P. F.; Strohriegl, P. *Phys. Rev. B* **1997**, *56*, 1269−1278.
(28) Alvarado, S. F.; Libioulle, L.; Seidler, P. F. *Synth. Met.* **1997**, *91*, 69−72.
(29) Liau, Y. H.; Scherer, N. F. *Proc. SPIE* **1998**, *3273*, 203−205.
(30) Briggs, D.; Seah, M. P. *Practical Surface Analysis*; John Wiley and Sons: New York, 1990.
(31) Moulder, D.; Sticle, W. F.; Sobol, P. E.; Bomben, K. D. *Handbook of Photoelectron Spectroscopy*; Physical Electronics Inc.: 1992.
(32) Cumpson, P. J.; Seah, M. P. *Surf. Interface Anal.* **1992**, *18*, 345−360.
(33) Mahl, S.; Neumann, M.; Schlett, V.; Baalmann, A. *Surf. Interface Anal.* **1998**, *22*, 204−212.
(34) Fowler, R. H.; Nordheim, L. *Proc. R. Soc. London, A* **1928**, *119*, 173.
(35) Glass, R. C.; Spellman, L. M.; Davis, R. F. *Appl. Phys. Lett.* **1991**, *59*, 2868.
(36) Park, Y.; Choong, V.; Gao, Y.; Hsieh, B. R.; Tang, C. W. *Appl. Phys. Lett.* **1996**, *68*, 2699.
(37) Sugiyama, K.; Ishii, H.; Ouchi, Y.; Seki, K. *J. Appl. Phys.* **2000**, *87*, 295−298.
(38) Cumpson, P. J.; Seah, M. P. *Surf. Interface Anal.* **1997**, *25*, 430−446.
(39) Kim, J. S.; Ho, P. K. H.; Thomas, D. S.; Friend, R. H.; Cacialli, F.; Bao, G. W.; Li, S. F. Y. *Chem. Phys. Lett.* **1999**, *315*, 307−312.
(40) Purvis, K. L.; Lu, G.; Schwartz, J.; Bernasek, S. L. *J. Am. Chem. Soc.* **2000**, *122*, 1808−1809.
(41) Wagner, C. D. *NIST XPS Database*; NIST: Washington, DC, 1989.